An in-frame deletion mutation in the degron tail of auxin coreceptor *IAA2* confers resistance to the herbicide 2,4-D in *Sisymbrium orientale*

Marcelo R. A. de Figueiredo[a], Anita Küpper[a,b], Jenna M. Malone[c], Tijana Petrovic[c], Ana Beatriz T. B. de Figueiredo[a], Grace Campagnola[d], Olve B. Peersen[d], Kasavajhala V. S. K. Prasad[e,f], Eric L. Patterson[a,g], Anireddy S. N. Reddy[e,f], Martin F. Kubeš[h], Richard Napier[h], Franck E. Dayan[a,f], Christopher Preston[c], and Todd A. Gaines[a,f,1]

[a]Department of Agricultural Biology, Colorado State University, Fort Collins, CO 80523; [b]Division CropScience, Weed Control Research, Bayer AG, 65926 Frankfurt, Germany; [c]School of Agriculture, Food and Wine, University of Adelaide, Adelaide, SA 5064, Australia; [d]Department of Biochemistry and Molecular Biology, Colorado State University, Fort Collins, CO 80523; [e]Department of Biology, Colorado State University, Fort Collins, CO 80523; [f]Program in Cell and Molecular Biology, Colorado State University, Fort Collins, CO 80523; [g]Department of Plant, Soil, and Microbial Sciences, Michigan State University, East Lansing, MI 48824; and [h]School of Life Sciences, The University of Warwick, Coventry, CV4 7AL, United Kingdom

Edited by Sean Cutler, University of California, Riverside, CA; received March 25, 2021; accepted December 9, 2021

The natural auxin indole-3-acetic acid (IAA) is a key regulator of many aspects of plant growth and development. Synthetic auxin herbicides such as 2,4-D mimic the effects of IAA by inducing strong auxinic-signaling responses in plants. To determine the mechanism of 2,4-D resistance in a *Sisymbrium orientale* (Indian hedge mustard) weed population, we performed a transcriptome analysis of 2,4-D-resistant (R) and -susceptible (S) genotypes that revealed an in-frame 27-nucleotide deletion removing nine amino acids in the degron tail (DT) of the auxin coreceptor Aux/IAA2 (*SoIAA2*). The deletion allele cosegregated with 2,4-D resistance in recombinant inbred lines. Further, this deletion was also detected in several 2,4-D-resistant field populations of this species. *Arabidopsis* transgenic lines expressing the *SoIAA2* mutant allele were resistant to 2,4-D and dicamba. The IAA2-DT deletion reduced binding to TIR1 in vitro with both natural and synthetic auxins, causing reduced association and increased dissociation rates. This mechanism of synthetic auxin herbicide resistance assigns an in planta function to the DT region of this Aux/IAA coreceptor for its role in synthetic auxin binding kinetics and reveals a potential biotechnological approach to produce synthetic auxin-resistant crops using gene-editing.

TIR1/AFB | dicamba | herbicide resistance | plant hormones | target-site resistance

The natural auxin indole-3-acetic acid (IAA) regulates developmental processes in plant growth and morphogenesis. Synthetic auxin herbicides mimic the effects of IAA and induce strong changes in gene expression that ultimately lead to lethal plant growth responses. Auxin Response Factors (ARF) are transcription factors that bind to the promoter regions of auxin-responsive genes (1). ARFs are regulated by transcriptional repressors called Auxin/INDOLE-3-ACETIC ACID (Aux/IAA) proteins, which are rapidly degraded upon auxin binding by a class of SKP1/CULLIN1/F-BOX PROTEIN (SCF) protein complexes that contain an F-box protein coreceptor family called Transport Inhibitor Response 1 and its analogous Auxin Signaling F-boxes (TIR1/AFBs). Auxins act as a "molecular glue" to bring together $SCF^{TIR1/AFB}$ and Aux/IAA. This process leads to Aux/IAA ubiquitination and subsequent degradation by the 26S proteasome, activating ARFs and the rapid transcription of auxin early responsive genes (2, 3).

Aux/IAA proteins have four motifs, including motif I for transcriptional repression, motif II consisting of the degron motif, a 13–amino acid sequence that binds to $SCF^{TIR1/AFB}$ and auxin, and motifs III and IV that forms a Phox and Bem1p (PB1 domain), which has homology to the PB1 domain of ARFs allowing the formation of homo and heterodimers that lead to transcriptional repression (4). The PB1 domain within Aux/IAAs has a resolved crystal structure (4), while the other motifs are characterized as intrinsically disordered regions (IDR) (5). Mutations in certain regions of Aux/IAA genes including the degron can lead to auxin insensitivity, producing strong phenotypes with changes in leaf shape, plant size, root development, underdeveloped reproductive systems, and low seed production (6, 7). A mutation causing a Gly127Asn amino acid substitution in the degron motif of the *Aux/IAA16* gene in the weed species *Bassia scoparia* conferred robust resistance to the synthetic auxin herbicide dicamba (8) but not cross-resistance to 2,4-dichlorophenoxyacetic acid (2,4-D) or fluroxypyr (9). This mutation also caused substantial growth defects and reduced competitiveness (9), showing the consequential

Significance

Synthetic auxin herbicides intersect basic plant developmental biology and applied weed management. We investigated resistance to 2,4-D in the Australian weed *Sisymbrium orientale* (Indian hedge mustard). We identified a mechanism involving an in-frame 27-bp deletion in the degron tail of auxin coreceptor IAA2, one member of the gene family of Aux/IAA auxin co-receptors. We show that this deletion in IAA2 is a gain-of-function mutation that confers synthetic auxin resistance. This field-evolved mechanism of resistance to synthetic auxin herbicides confirms previous biochemical studies showing the role of the Aux/IAA degron tail in regulating Aux/IAA protein degradation upon auxin perception. The deletion mutation could be generated in crops using gene-editing approaches for cross-resistance to multiple synthetic auxin herbicides.

Author contributions: M.R.A.d.F., A.K., J.M.M., O.B.P., E.L.P., A.S.N.R., R.N., C.P., and T.A.G. designed research; M.R.A.d.F., A.K., J.M.M., T.P., A.B.T.B.d.F., G.C., K.V.S.K.P., E.L.P., M.F.K., R.N., and F.E.D. performed research; G.C., O.B.P., A.S.N.R., R.N., and C.P. contributed new reagents/analytic tools; M.R.A.d.F., A.K., J.M.M., G.C., K.V.S.K.P., E.L.P., M.F.K., R.N., F.E.D., and T.A.G. analyzed data; and M.R.A.d.F., A.K., J.M.M., T.P., A.B.T.B.d.F., G.C., O.B.P., K.V.S.K.P., E.L.P., A.S.N.R., M.F.K., R.N., F.E.D., C.P., and T.A.G. wrote the paper.

Competing interest statement: A pending patent application related to the use of the IAA2 mutation to generate herbicide-resistant plants has been filed by Colorado State University Foundation and University of Adelaide for inventors T.A.G., M.R.A.F., A.K., and C.P. and application number WO2020185907A1.

This article is a PNAS Direct Submission.

[1]To whom correspondence may be addressed. Email: todd.gaines@colostate.edu.

This article contains supporting information online at http://www.pnas.org/lookup/suppl/doi:10.1073/pnas.2105819119/-/DCSupplemental.

Published February 25, 2022.

implications of mutations in the degron motif of Aux/IAA proteins. Currently, 41 different weed species have evolved resistance to synthetic auxin herbicides (10). Herbicide-resistance mechanisms involve mutations in the gene encoding the target-site protein(s) as well as nontarget site changes to alter herbicide movement or rate of degradation to nonphytotoxic forms (11). Synthetic auxin herbicide–resistant weeds have been reported to have rapid metabolic degradation of the herbicide (12), reduced herbicide translocation to the growing point (13, 14), and increased expression of transmembrane kinase and receptor proteins (15). Except for the *IAA16* Gly127Asn degron mutation, the causative molecular basis of evolved synthetic auxin resistance in weeds is unknown (11, 16).

In 2005, a population of the weed species *Sisymbrium orientale* (Indian hedge mustard) was reported to be resistant to the synthetic auxin herbicides 2,4-D and 2-methyl-4-chlorophenoxyacetic acid in South Australia (17). In the resistant population, 2,4-D translocation was reduced (18), and progeny tests revealed that the resistance was inherited as a single dominant allele (19). Given the importance of synthetic auxins to agriculture and the recent introduction of engineered resistance to 2,4-D and dicamba in soybean and cotton (20, 21), we investigated the mechanism of 2,4-D resistance in natural populations of the weed *S. orientale*. We performed a transcriptome analysis on recombinant inbred lines (RILs) derived from a cross between 2,4-D-resistant (R) and -susceptible (S) genotypes and found an in-frame 27-bp deletion in the degron tail (DT) of the auxin coreceptor Aux/IAA2 (*SoIAA2*). This loss of nine amino acids due to DT deletion reduced binding of both natural and synthetic auxins to TIR1 and conferred cross-resistance to 2,4-D and dicamba, thus indicating the role of IAA2 in auxin perception and revealing the significance of the DT region in Aux/IAA degradation. These results demonstrate a resistance mechanism that confers field-evolved synthetic auxin herbicide resistance, advances our understanding of Aux/IAA motif functionality in auxin perception and signaling, and identifies a biotechnological tool that can be achieved by gene-editing rather than transgene insertion for production of synthetic auxin-resistant crops.

Results

Identification of *IAA2* as a Candidate Gene for Herbicide Resistance through RNA-Sequencing. The transcriptomes of untreated *S. orientale* plants were sequenced, consisting of six F4 RILs derived from a cross between 2,4-D-resistant PB-R (Port Broughton–Resistant) and susceptible S (Cross A, 3 R-RILs and 3 S-RILs) and six F3 RILs from a cross between 2,4-D-resistant PB-R2 and susceptible S (Cross B, two R-RILs, and four S-RILs). Average reads per sample were 6.7×10^7 with >40 quality control score. Only one transcript, *SoIAA2*, had differential expression between R-RILs and S-RILs of both PB-R and PB-R2 populations based on cutoff criteria of false discovery rate (FDR) <0.05, fold change of > |2|, and a consistent expression pattern in all R-RIL replicates compared to all S-RIL replicates. The IAA2 protein encoded by *SoIAA2* (3.3-fold lower expression in R than S, FDR < 0.0001) showed a high-sequence similarity to the *Arabidopsis* IAA2 protein encoded by AT3G23030 (*SI Appendix*, Fig. 1). No single-nucleotide changes in any transcripts were identified that were shared among all R-RILs and different from all S-RILs. Inspection of the read alignments to *SoIAA2* identified a gap in read coverage for all R-RILs, suggesting a deletion in the R allele, whereas all S-RILs had continuous read coverage at this position (*SI Appendix*, Fig. 2). Transcriptome analysis led to the hypothesis that resistance was linked to this deletion mutation in *SoIAA2*.

***SoIAA2* Gene-Sequencing.** A 239-bp region of the *SoIAA2* gene that includes the predicted deletion was amplified and sequenced from three R-RILs and three S-RILs. The 27-bp deletion in the R allele (gene and messenger RNA [mRNA] referred to as $SoIAA2_{\Delta 27}$) was confirmed (Fig. 1*A*). The deletion results in an in-frame protein lacking nine amino acids (aa 73 through 81; protein referred to as $So\text{IAA2}_{\Delta 9}$) comprising most of the DT region between the degron and the PB1 domain (Fig. 1*A*). None of the S-RILs contained a deletion in *SoIAA2*, showing that the deletion was correlated with resistance.

The presence of $SoIAA2_{\Delta 27}$ in other 2,4-D resistant populations of *S. orientale* was investigated. Eight populations from South Australia, including parent populations PB-R and PB-R2 were screened for resistance to 2,4-D, with four populations identified as resistant. The *SoIAA2* gene was sequenced to determine the presence or absence of $SoIAA2_{\Delta 27}$ in individual plants from each population (*SI Appendix*, Table 1). Full-length *SoIAA2* was present in individuals from four susceptible populations, P15, P31, P49, and P50. All individuals from the two parent-resistant populations, PB-R and PB-R2, contained $SoIAA2_{\Delta 27}$. Individuals from resistant population P17 were found to be homozygous for $SoIAA2_{\Delta 27}$, or heterozygous for $SoIAA2_{\Delta 27}$ and wild-type (WT) *SoIAA2*, suggesting a segregating population for this locus. Population P28, although resistant, did not contain $SoIAA2_{\Delta 27}$, suggesting a different synthetic auxin herbicide–resistance mechanism may have evolved in this population. Overall, sequence data identified a 27-base pair deletion in *SoIAA2* as the candidate mutation associated with resistance to 2,4-D in several *S. orientale* populations from Port Broughton, Australia.

Segregation of $SoIAA2_{\Delta 27}$. The heritable association between $SoIAA2_{\Delta 27}$ and the resistance phenotype (evaluated as visual injury on a scale of 0 to 100%) was confirmed by forward genetics through segregation and genotyping analysis. Susceptible progeny of a self-pollinated heterozygous individual (70% visual injury after 250 g/active ingredient [ai]/ha^{-1} 2,4-D treatment) were homozygous for WT *SoIAA2*, heterozygous offspring showed an average of 24% injury, and resistant plants (average 12% injury) were homozygous for $SoIAA2_{\Delta 27}$ (Fig. 1*B*). Therefore, the resistance phenotype segregates with the mutant allele $SoIAA2_{\Delta 27}$. Relative expression of auxin-responsive genes *IAA2*, *IAA19*, and *GH3.3* was compared between R and S plants after 250 g/ai/ha^{-1} 2,4-D treatment. In untreated plants, *GH3.3* and *IAA19* had no detectable transcripts for both genotypes, while *SoIAA2* had low expression (Fig. 1*C*). Both S and R plants had similar increased *GH3.3* expression levels after 2,4-D treatment; however, relative expression of both *IAA19* and *IAA2* increased in S while expression in R did not increase following 2,4-D treatment (Fig. 1*C*).

Evaluation of Potential Nontarget Site Mechanisms of Auxin Resistance. To rule out other potential herbicide-resistance mechanisms not related to the Aux/IAA candidate, experiments using [14C] 2,4-D were performed to evaluate differences in herbicide absorption, translocation, and metabolism between R and S populations. There were no differences in maximum herbicide absorption (A_{max} R: 91% ± SE 0.8% and S: 92% ± SE 0.8%) or time for 90% of maximum herbicide absorption (T_{90} R: 2.9 h ± SE 0.3 h and S: 3.5 h ± SE 0.2 h) between populations (*SI Appendix*, Fig. 3*A* and Table 2). Herbicide translocation was low for both genotypes (A_{max} - S: 6.5% ± SE 2.5% and R: 14.3% ± SE 2.6%; T_{90} - S: 105 h; and R: 119 h). R plants had higher herbicide translocation as measured by A_{max} (*P* value: 0.036), but T_{90} was similar (*SI Appendix*, Fig. 3 *B* and *C* and Table 2). For herbicide metabolism quantification in plant lysates, the parent compound of [14C] 2,4-D was detected at 13.4 min by reverse-phase high-performance liquid chromatography (HPLC), and it was maintained as the predominant

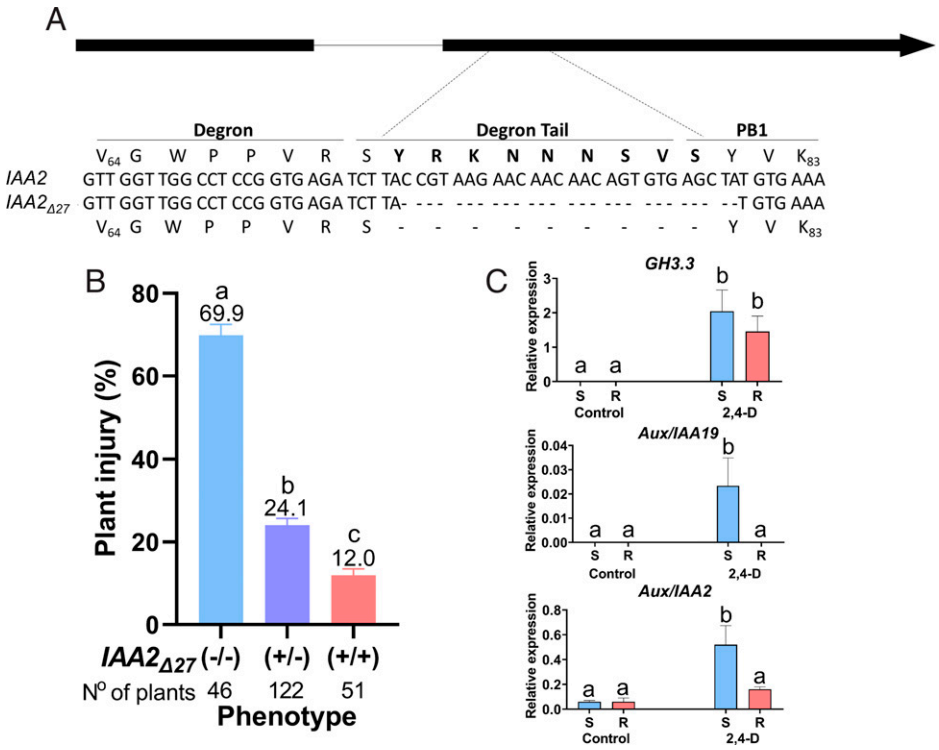

Fig. 1. A deletion in *SoIAA2* confers resistance to 2,4-D. Deletion of 27 nucleotides from the *S. orientale IAA2* gene results in a nine–amino acid deletion in the DT region of IAA2. (*A*) *SoIAA2* schematic representation with two exons (black boxes) and one intron (line). Sequences show differences between susceptible, S (*IAA2*) and resistant, R ($IAA2_{\Delta 27}$) alleles, and dashed lines show the nucleotides and amino acids that were deleted in the R allele. (*B*) The deletion allele segregates with 2,4-D resistance in an F_2 population. Plants were genotyped for the *IAA2* R and S alleles then sprayed with 250 gai/ha^{-1} 2,4-D and evaluated for plant injury 28 d after treatment. Different letters indicate differences between means ($P < 0.05$). (*C*) Effect of 2,4-D treatment on genes related to auxin responses, *SoGH3.3*, *SoIAA19*, and *SoIAA2*. Herbicide treatment induces higher expression in S compared to R lines for *SoIAA19* and *SoIAA2* but not *SoGH3.3*. Different letters indicate differences between means ($P < 0.05$). Plants were sprayed with 250 g/ai/ha^{-1} 2,4-D, and relative gene expression was measured after 6 h using qRT-PCR with *cyclophilin* and *actin2* as normalization genes ($n = 3$ plants). Error bars correspond to SD.

radiolabeled compound for both populations at all time points (*SI Appendix*, Fig. 3*D* and Table 2). The half-life of 2,4-D in R plants (200 h ± SE 22) and S plants (118 h ± SE 42) could not account for the difference in phenotype. Taken together, these results indicate that changes in absorption, translocation, and metabolism are not the mechanism of 2,4-D resistance in this R population.

Expression of *So*IAA2$_{\Delta 27}$ in *Arabidopsis* Confers 2,4-D and Dicamba Resistance. To test whether $SoIAA2_{\Delta 27}$ was sufficient to confer 2,4-D resistance, *Arabidopsis* was transformed with an empty *pFGC5941* vector (∅), *SoIAA2*, and $SoIAA2_{\Delta 27}$ under the *CaMV35S* promoter (*SI Appendix*, Fig. 4). Genotypes were confirmed by PCR, and plants containing the empty vector and WT *SoIAA2* did not show obvious changes in plant phenotype (Fig. 2*A*). *Arabidopsis*-transformed lines that were heterozygous for $SoIAA2_{\Delta 27}$ had lanceolate shape leaves and a minor reduction in plant size. Plants homozygous for $SoIAA2_{\Delta 27}$ had strong morphological abnormalities, dwarfism, a reduced number of reproductive organs, and lower seed production. Total biomass of transformed plants homozygous for $SoIAA2_{\Delta 27}$ was substantially lower compared to Col-0 and lines transformed with *SoIAA2* or a null vector (Fig. 2*A*).

A root-growth assay in the presence and absence of IAA and synthetic auxins was performed using the transformed *Arabidopsis* lines. Col-0 (WT) and plants containing the null vector (∅2 and ∅4) and *SoIAA2* (S1 and S7) were susceptible to 2,4-D (0.5 μM) and dicamba (20 μM), with root elongation of 5 to 6% relative to the ethanol control in the presence of 2,4-D and root elongation of 10 to 13% relative to the ethanol control in the presence of dicamba (Fig. 2*B*). *Arabidopsis* transformed with $SoIAA2_{\Delta 27}$ (lines R1 and R4) exhibited resistance to 2,4-D and dicamba, with root elongation of 24% and 36% relative to the ethanol control for 2,4-D and root elongation of 25% and 42% relative to the ethanol control for dicamba (Fig. 2*B*). R4 $SoIAA2_{\Delta 27}$ was resistant to IAA, with 77% root elongation compared to the ethanol control. All other lines were sensitive to IAA at 0.5 μM, including Col-0, empty vector lines, lines expressing *SoIAA2* (S1 and S7), and line R1. $SoIAA2_{\Delta 27}$-expressing lines were also resistant to 2,4-D and dicamba at the whole-plant level with foliar herbicide applications (*SI Appendix*, Fig. 5 and Table 3). The auxin-responsive genes *AtIAA19* and *AtGH3.3* exhibited an increase in expression levels following 2,4-D foliar treatment in Col-0, null vector (Ø2), and *SoIAA2* (S1 and S7) lines, while lines transformed with $SoIAA2_{\Delta 27}$ (R1 and R4) showed no increase in expression of *AtIAA19* and *AtGH3.3* following 2,4-D treatment (Fig. 2*C*). *AtIAA2* expression was similar to that of Col-0 and null vector lines. Taking all these results together, $SoIAA2_{\Delta 27}$ is sufficient to confer resistance to both 2,4-D and dicamba when expressed in *Arabidopsis*.

***So*IAA2 and *So*IAA2$_{\Delta 9}$ Protein Structure.** The Aux/IAA DT has previously been shown to be critical for the Aux/IAA interaction with TIR1, facilitating the ubiquitination of the PB1 domain (5). Compared to other Aux/IAA proteins, *So*IAA2 has a shorter and relatively structured DT. The nine–amino acid deleted section of the DT is hydrophilic, and in silico models predict the deleted DT region and the PB1 domain to be predominantly structured and rigid (*SI Appendix*, Fig. 6). To examine structural changes induced

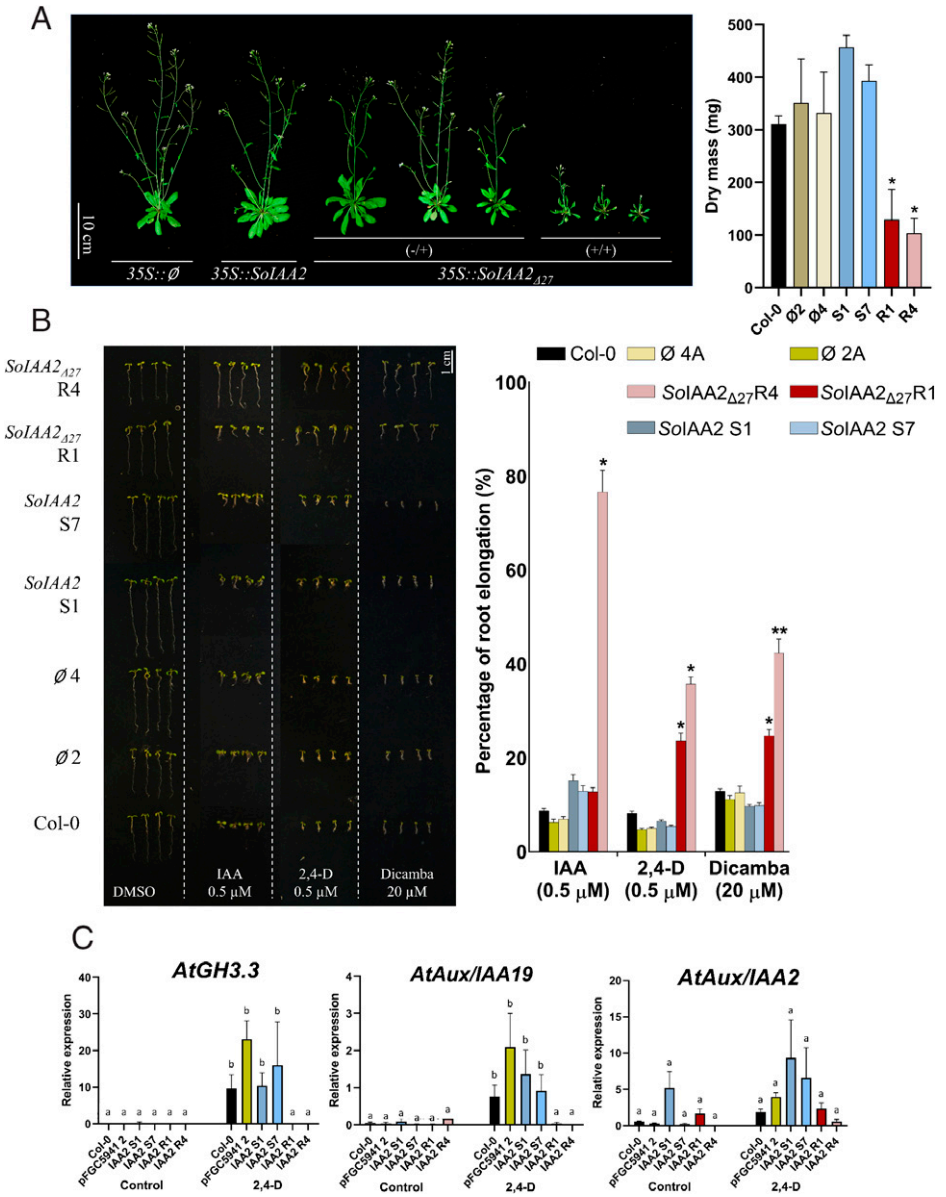

Fig. 2. Transformation of *A. thaliana* with the *IAA2* wild-type allele and $IAA2_{\Delta 27}$ allele from *S. orientale*. Treatments with the auxin herbicides 2,4-D and dicamba result in different root-growth and gene-expression responses consistent with the hypothesis that the $IAA2_{\Delta 27}$ allele confers resistance. (*A*, *Left*) Pictures of transgenic lines 28 d after germination. Lines with vector control (35S::∅), *IAA2* (35S::*So*IAA2), and $IAA2_{\Delta 27}$ (35S::*So* $IAA_{\Delta 27}$) are shown. The symbols +/− correspond to heterozygous and +/+ correspond to homozygous plants. Pictures are representative of at least three transformed lines selected for glufosinate resistance. (*Right*) Dry mass data at 28 d after germination. Statistical significance between treatments is represented by asterisks; error bars are ± SD ($n = 3$, P value ≤ 0.05). (*B*) Only the $IAA2_{\Delta 27}$ allele grows on media containing auxin herbicides. (*Left*) Representative photos of seedlings of Col-0 (WT) and two independent lines for each (∅), *IAA2*, and $IAA_{\Delta 27}$ constructs growing on agar plates of auxins or the same final concentration of ethanol as control 7 d after germination. (*Right*) Root elongation data. Error bars correspond to SE. Asterisks correspond to statistical significances between different treatments ($n \leq 50$ plants; P value ≤ 0.05). (*C*) Gene expression of auxin-responsive genes *AtGH3.3* and *AtAux/IAA19* increased at 6 h after 2,4-D postemergence treatment in *Arabidopsis* Col-0, empty vector (pFGC5941 2), and transgenic lines expressing wild-type *IAA2* (35S::*SoIAA2*; *SoIAA2* S1 and S7), while no gene-expression increase occurred in transgenic lines expressing $IAA2_{\Delta 27}$ (35S::$SoIAA_{\Delta 27}$; *SoIAA2* R1 and R4) ($n = 3$). Different letters indicate differences between means (for *AtGH3.3*, $P < 0.05$; for *AtAux/IAA19*, $P < 0.1$), and error bars correspond to SD. No significant gene-expression changes occurred for *AtAux/IAA2* 6 h after 2,4-D post-emergence treatment.

by the deletion mutation, full-length *So*IAA2 and $SoIAA2_{\Delta 9}$ (the protein product of $SoIAA2_{\Delta 27}$) were expressed and purified to perform circular dichroism (CD) spectrometry and size-exclusion chromatography. Size-exclusion chromatography showed that both mutant and wild-type proteins purify as oligomers of varied composition depending on protein concentration (*SI Appendix*, Fig. 7 *A* and *B*), which has also been seen for other Aux/IAA proteins (22, 23). While the deletion did not disrupt or enhance oligomer formation, it did enhance the overall stability of the protein. During the purification process, the wild-type protein displayed a much-lower maximum-concentration threshold than the deletion mutation (*SI Appendix*, Fig. 7*A*). CD spectrometry data are nearly identical for both proteins (*SI Appendix*, Fig. 7*D*). A BeStSel analysis of the data (24) results in an alpha:beta:other content of 13%:38%:49%, which agrees with a partial structure from the PB1 domain and about half of the protein being disordered or "other." This suggests the nine–amino acid deletion does not impact the overall folding of the protein (*SI Appendix*, Fig. 7*D*).

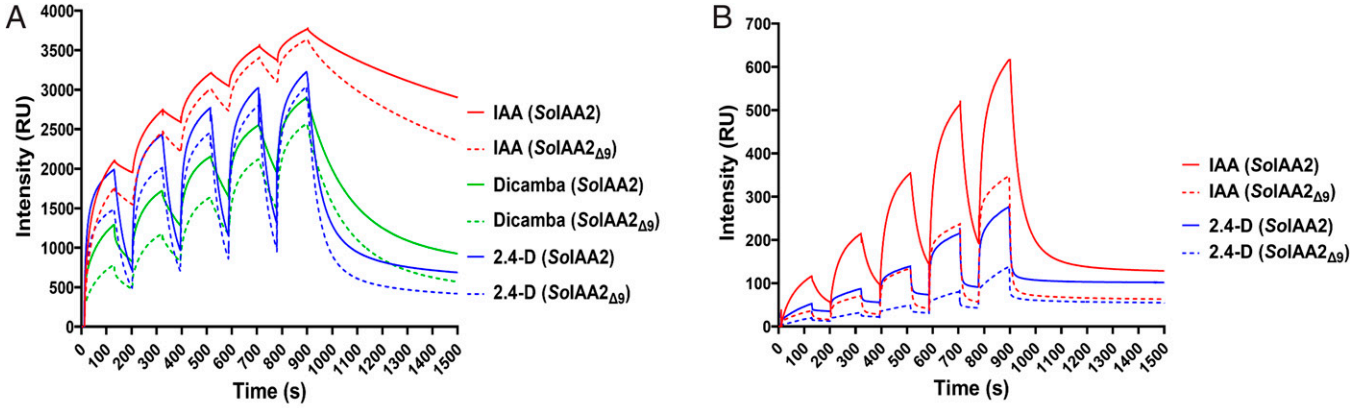

Ligand	Auxin	k_a (M^{-1} s^{-1})	k_d (s^{-1})	K_D (nM)
TIR1-*So*IAA2$_{\Delta 9}$	IAA	1.23E+04	5.01E-04	41
TIR1-*So*IAA2	IAA	1.83E+04	2.08E-04	11
TIR1-*So*IAA2$_{\Delta 9}$	2,4-D	1.11E+05	3.29E-02	300
TIR1-*So*IAA2	2,4-D	3.01E+05	4.04E-02	140
TIR1-*So*IAA2$_{\Delta 9}$	Dicamba	3.90E+03	2.71E-03	700
TIR1-*So*IAA2	Dicamba	7.71E+03	1.93E-03	250

Ligand	Auxin	k_a (M^{-1} s^{-1})	k_d (s^{-1})	K_D (nM)
AFB5-*So*IAA2$_{\Delta 9}$	IAA	4.35E02	1.10E-3	2500
AFB5-*So*IAA2	IAA	9.19E02	3.26E-3	3500
AFB5-*So*IAA2$_{\Delta 9}$	2,4-D	No fit		
AFB5-*So*IAA2	2,4-D	No fit		

Fig. 3. The mutant *So*IAA2$_{\Delta 9}$ binds to the receptors TIR1 and AFB5 with poorer affinity than the WT *So*IAA2. SPR was used to measure the binding of purified receptor protein to each degron peptide using single-cycle kinetics. (*A*) Typical sensorgrams showing binding and dissociation of TIR1 with each degron peptide at a series of rising concentrations of each auxin. (*B*) The same analysis with AFB5, which characteristically displays faster kinetics for both association of the complex, and dissociation is shown. Auxins were mixed with the TIR1 or AFB5 preparation in advance of injection over the biotinylated *So*IAA2 peptides using standard Biacore double-baseline subtraction with single-cycle kinetic routines. RU, resonance units. Tables show kinetic data for the binding of TIR1 (*Left*) and AFB5 (*Right*) to *So*IAA2 and *So*IAA2$_{\Delta 9}$ in the presence of natural and synthetic auxins. Values were calculated using a global fit for a Langmuir 1:1 kinetic model using the manufacturer's BiaEvaluation software.

Binding-Affinity Analysis of TIR1/AFB with *So*IAA2 and *So*IAA2$_{\Delta 9}$. To determine the mechanism by which the DT deletion in *So*IAA2 interferes with synthetic auxin herbicide–binding, a surface plasmon resonance (SPR) assay was performed (25). The assay measures the auxin-induced assembly of TIR1/AFB receptors with degron peptides, which is representative of the coreceptor complex (26). We used a biotinylated 24-aa peptide (*So*IAA2) consisting of the degron core (9 aa), DT (9 aa), a small fraction of PB1 (6 aa), and a biotinylated 15-aa peptide lacking the DT segment (*So*IAA2$_{\Delta 9}$) (*SI Appendix*, Table 4). Both peptides bound to TIR1 and to AFB5 in the presence of IAA (Fig. 3 *A* and *B*). However, the assay showed weaker binding by *So*IAA2$_{\Delta 9}$ to TIR1 with IAA compared to WT *So*IAA2 and similarly weaker binding with both synthetic auxins 2,4-D and dicamba (Fig. 3). Binding kinetic experiments showed that weaker binding translates as lower affinity (a higher equilibrium dissociation constant, K_D) for *So*IAA2$_{\Delta 9}$ than for *So*IAA2 in each TIR1-auxin complex (K_D IAA, 41 versus 11 nM; 2,4-D, 300 versus 140 nM; and dicamba, 700 versus 250 nM). The association-rate constants (k_a) of *So*IAA2$_{\Delta 9}$ were always lower than for WT *So*IAA2 in association with TIR1 (Fig. 3*A*). The dissociation-rate constants (k_d) were higher for the TIR1–*So*IAA2$_{\Delta 9}$ complex with IAA and dicamba but were slightly lower for 2,4-D with the TIR1–SoIAA2$_{\Delta 9}$ complex (Fig. 3*A*). The kinetic data suggest that the lower affinity binding of the mutant will be slower to form and be less stable in the coreceptor complex in the presence of both auxin and synthetic auxin herbicides. The potential consequences of this lower affinity binding could include reduced ubiquitination, longer lifetimes of Aux/IAA proteins, and reduced sensitivity to auxins.

Homology-Based Modeling and Docking Analysis for TIR1 with *So*IAA2 and *So*IAA2$_{\Delta 9}$. Homology-based protein models were used to explore the effect of the DT deletion on the interaction between TIR1 and *So*IAA2. The sequence of IAA7 (chain C of Protein Data Bank [PDB]: 2P1Q) (2) had 85% sequence identity to the corresponding sequence of *So*IAA2 and included no gaps. The crystal structure of pea (*Pisum sativum*) PB1 domain (PDB: 2M1M) (4) was identified as a crystal homolog of the PB1 portion of *So*IAA2 using the search function of Swiss Model (27). Sequence comparison revealed a 72% sequence identity with no gaps. Docking of *So*IAA2 and *So*IAA2$_{\Delta 9}$ models generated several clusters (*SI Appendix*, Table 5). Clusters 3 and 1 had the lowest z-score for *So*IAA2 and *So*IAA2$_{\Delta 9}$, respectively (*SI Appendix*, Table 5). Docking of *So*IAA2 to TIR1 was better than that of *So*IAA2$_{\Delta 9}$, with a 25% reduction in affinity for *So*IAA2$_{\Delta 9}$ ($\Delta G = -8$ kCal/mol^{-1}; SD $\pm$ 0.55) relative to *So*IAA2 ($\Delta G = -10.63$ kCal/mol^{-1}; SD $\pm$ 0.64) and a 160-fold decrease in the dissociation constant for *So*IAA2$_{\Delta 9}$ (K_D = 5 μM; SD $\pm$ 1.74) relative to *So*IAA2 (K_D = 0.031 μM; SD $\pm$ 0.005) (Fig. 4*A*). Docking of *So*IAA2 allowed for interaction of PB1 with TIR1 as described by Niemeyer et al. (5), while maintaining the same interaction of the core IAA2 degron toward the center of the barrel described by Tan et al. (2). On the other hand, the deletion of nine residues in *So*IAA2$_{\Delta 9}$ caused a dramatic change in the architecture of IAA2 that preserved the degron's ability to interact with TIR1 while preventing the proper interaction of PB1 with its binding domain on the outside of TIR1 (Fig. 4*B*). Overall, we propose that in the presence of auxin, the WT version of *So*IAA2 binds to TIR1 by interacting with the degron and the PB1 domain. In this conformation, the IDR is displayed across the top surface of TIR1 with all lysine residues accessible for ubiquitination. In *So*IAA2$_{\Delta 9}$-resistant individuals, the reduction of the molecular distance between the core degron and the PB1 domain likely precludes binding of this domain to TIR1. Lower overall affinity for *So*IAA2$_{\Delta 9}$ may reduce the lifetime of the complex and reduce the likelihood of polyubiquitination (Fig. 4*C*).

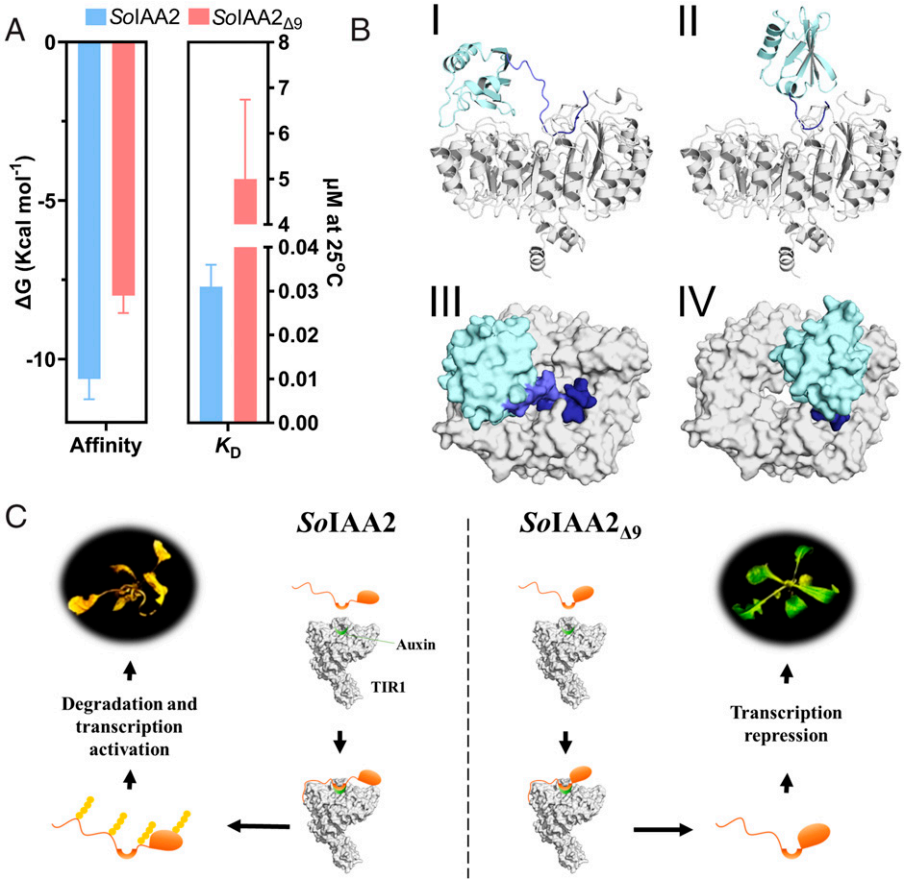

Fig. 4. DT deletion in *So*IAA2$_{\Delta 9}$ alters PB1 domain association to the TIR1/auxin complex and decreases binding affinity. (*A*) Computational characterization of the thermodynamic profiles of *So*IAA2 and *So*IAA2$_{\Delta 9}$ docking to TIR1. Binding free-energy ΔG and dissociation constant K_D were calculated. (*B*) Docking of *So*IAA2 and *So*IAA2$_{\Delta 9}$ to TIR1. Side view of the interaction between TIR1 (white) and I) *So*IAA2 and II) *So*IAA2$_{\Delta 9}$ is shown (proteins are displayed as cartoons). Bird's eye view of the interaction between TIR1 (white) and III) *So*IAA2 and IV) *So*IAA2$_{\Delta 9}$ is shown (proteins are displayed as surfaces). The different parts of *So*IAA2 are shown as light blue for PB1, blue for the nine residues that are deleted in *So*IAA2$_{\Delta 9}$ (DT), and dark blue for the *So*IAA2 core degron. Panels II and IV are drawn with the degron instead of the PB1 domain bound, because it had the more-favorable, calculated binding energy, and this pose is therefore predicted to be more likely. (*C*) Proposed hypothetical model for the mechanistic basis of 2,4-D resistance caused by the DT deletion in *So*IAA2$_{\Delta 9}$ due to altered association with the TIR1/2,4-D/IAA2 protein complex. (*Left*) In the WT *So*IAA2 protein, the degron binds to TIR1 with auxinic herbicides resulting in ubiquitination and degradation of *So*IAA2 by the 26S proteasome, inducing transcriptional activation, which culminates in plant death. (*Right*) In the mutant *So*IAA2$_{\Delta 9}$ protein, the TIR1/AFB coreceptor may interact with the degron, but the loss of DT leads to fewer and shorter binding events that may reduce of the rate of *So*IAA2$_{\Delta 9}$ protein ubiquitination. Auxin-responsive genes are not induced by synthetic auxin herbicides, which leads to herbicide resistance.

Discussion

The target sites for synthetic auxin herbicides consist of complexes of two protein families, the receptor TIR1/AFB and the coreceptor Aux/IAA protein. The deletion of 27 nucleotides in the gene *SoIAA2* results in the loss of nine amino acids in the DT of *So*IAA2, which is a mechanism of target-site mutation in the auxin coreceptor associated with resistance to auxin herbicides in weeds. Our results confirm the importance of the DT as a contributor to Aux/IAA stability (5) and for perception of synthetic auxin herbicides in planta. Homology modeling indicated that the *So*IAA2$_{\Delta 9}$ protein is only able to engage one of the two domains (PB1 and the degron) at a time when binding to TIR1/AFB (Fig. 3). A poorer binding affinity associated with an increased rate of dissociation for *So*IAA2$_{\Delta 9}$ compared to *So*IAA2 in the synthetic auxin/TIR1 receptor/IAA2 coreceptor interaction is likely the main explanation for herbicide resistance in this population of *S. orientale* (Figs. 3 and 4). The loss of a crucial lysine within the DT, K_{74}, could also contribute to the resistance phenotype. Equivalent residues in the DT of *At*IAA7 and *At*IAA12 were shown to be ubiquitinated in *Arabidopsis*, but because additional lysine residues are present in IAA2 DT (5), the loss of K_{74} alone is not likely to explain the phenotype. These additional lysine residues could be subject to steric hindrance that could limit lysine ubiquitination, since PB1 appears to occlude most of domain II (Fig. 4). Another putative explanation for the loss of sensitivity to auxins is increased oligomerization. *So*IAA2$_{\Delta 9}$ had increased in vitro stability forming higher oligomers compared to the wild-type *So*IAA2. ARF repression due to increased *So*IAA2$_{\Delta 9}$ oligomerization may also contribute to the resistance mechanism, because protein stability and oligomerization are important factors for transcription repression activity (28).

The DT deletion reduced the binding affinity of the mutant Aux/IAA coreceptor protein for the TIR1 receptor with all auxins tested in SPR binding assays (Fig. 3*A*). In silico molecular-docking analysis showed similar changes in the calculated binding kinetics to that measured in the biochemical assays (Fig. 4*A*). *So*IAA2 bound in a similar fashion as that proposed by Niemeyer et al. and Tan et al. (2, 5). The deletion of nine amino acids from the DT in *So*IAA2$_{\Delta 9}$ caused a dramatic change in the architecture of the protein, permitting the degron to continue to interact with TIR1 while preventing the proper interaction of PB1 (Fig. 4*B*). Thus, resistance may be associated with reduced binding of the mutant *So*IAA2$_{\Delta 9}$, resulting in less ubiquitination and subsequent degradation by the proteasome. We propose a hypothetical model to be tested in future work that the *So*IAA2$_{\Delta 9}$ protein maintains

higher transcriptional repression of auxin-responsive genes in the presence of synthetic auxin herbicides than wild-type *So*IAA2 (Fig. 4*C*). *So*IAA2 DT deletion leads to cross-resistance to both 2,4-D and dicamba, revealing a pathway to explore introduction of synthetic auxin resistance traits in crop plants by targeting the DT region using gene-editing technologies.

SoIAA2 had low expression under natural conditions; however, it was induced rapidly after exogenous auxin application. A similar response was also observed in *Arabidopsis* Col-0 seedlings, in which the expression of *AtIAA2* increased sixfold 1 h after 2,4-D treatment (29). The $SoIAA2_{\Delta 27}$ allele encoding the $SoIAA2_{\Delta 9}$ protein maintained transcriptional repression of auxin-responsive genes *GH3.3* and *IAA19* following 2,4-D treatment, showing that the DT is critical for IAA and synthetic auxin herbicide–binding, leading to Aux/IAA protein degradation. *So*IAA2 seems to play an important role in auxin perception. Previous reports of mutations that confer higher stability to Aux/IAA proteins have been associated with drastic morphological defects, as for *axr5-1*/IAA1 (30, 31), shy2/IAA3 (32), *axr2*/IAA7 (31), *iaa16* (6), and *iaa28* (33). All these mutants were reported to be insensitive or hypersensitive to natural and synthetic auxins. Further, in the weed species *B. scoparia*, a mutation in the core degron of *BsIAA16* conferred dicamba resistance but also resulted in a substantial fitness penalty in the form of reduced growth and competitiveness (8, 9). In our study, overexpression of $SoIAA2_{\Delta 27}$ in *Arabidopsis* induced strong phenotypes in homozygous plants with severely reduced growth (Fig. 2*A*). Future research is needed to determine whether the $SoIAA2_{\Delta 27}$ mutation in 2,4-D-resistant *S. orientale* causes any morphological or reproductive defects or reduction in competitiveness with crops.

Materials and Methods

Plant Material. One population of 2,4-D-resistant *S. orientale* was collected from a wheat field in Port Broughton (PB-R), and a second 2,4-D resistant population was collected 9.2 km away (PB-R2), while the susceptible population originated from Roseworthy (S), Australia (17, 19). Two biparental crosses were made to study inheritance of 2,4-D resistance (18), using PB-R as the male parent for Cross A and PB-R2 as the male parent for Cross B, with S as the female parent for both crosses. The F1 progeny were self pollinated to produce F2 progeny, and F2 individuals were self pollinated to produce F3 progeny (18, 19). Homozygous resistant and homozygous susceptible F3 lines were inbred via single-seed descent to create RILs to the F4 generation (Cross A). The F3 generation was used for Cross B.

RNA-Sequencing. RNA-sequencing (RNA-seq) was performed on untreated plants from a total of 12 individual RILs, including six individuals each from Cross A (three homozygous 2,4-D-resistant and three homozygous 2,4-D-susceptible) and Cross B (two homozygous 2,4-D-resistant and four homozygous 2,4-D-susceptible). RNA from the youngest expanded leaf of four-leaf stage plants was extracted using the RNeasy Plant Mini Kit (Qiagen), and libraries were prepared using the TruSeq Stranded mRNA Sample Prep Kit (Illumina). Sequencing was performed on a HiSeq 4000 (Illumina) using bar-coded adapters in two lanes of the Illumina flow cell for 101 cycles, yielding 1.6 billion paired-end reads. Individual library yields ranged from 52 to 75 million paired-end reads. Fastq files were generated and demultiplexed with bcl2fastq version 2.17.1.13 conversion software (Illumina), and adaptors were trimmed from the 3′-end reads. The sequence data and processed data files discussed in this publication are deposited in National Center for Biotechnology Information (NCBI's) Gene Expression Omnibus (GEO) (34) and accessible through GEO Series accession no. GSE159202 (https://www.ncbi.nlm.nih.gov/geo/query/acc.cgi?acc=GSE159202).

A de novo reference transcriptome was obtained by separately assembling Illumina reads from a Cross A 2,4-D-resistant RIL (R206) and a susceptible RIL (S242) with Trinity (35). The assembled contigs were filtered for minimum contig length of 500 bp. The two assemblies were compared and merged using CDHit version 4.6.6 (35) with a 95% CI to eliminate redundant contigs and retain all contigs unique to either the R or S assembly. This resulted in a 72-Mb transcriptome with 40,987 contigs (available at GEO Series accession no. GSE159202) (BUSCO score of 98.4%, Eukaryota ODB10). Putative annotations were assigned using Trinotate (36) and The Arabidopsis Information Resource (TAIR) 10 protein database (37). Read alignments to the de novo reference transcriptome were conducted with Bowtie2 (38) using the default "end-to-end" mode and the "sensitive" option. The minimum allowed fragment length was set to 100 and the maximum to 800 bp.

Differential Expression and Single-Nucleotide Polymorphism Analysis. Raw read counts were extracted using sequence alignment/map (SAMtools) (39). Counts-per-million (CPM) and gene-expression differences were calculated with the package "edgeR" (40) using the statistical software R version 3.3 (41) and an expression threshold of ≥1 CPM in at least two samples. After normalization expression differences were compared between 2,4-D resistant and susceptible RILs within Cross A and B, respectively, as well as between all 2,4-D-resistant and -susceptible RILs. Differentially expressed transcripts were then filtered for a fold change of $\geq |2|$ and an FDR adjusted P value ≤ 0.05. Transcripts annotated as PRP39-2 (10-fold lower in R than S, FDR < 0.0001, similar to AT5G46400 that encodes for tetratricopeptide repeat [TPR-like] superfamily protein) and ABCB13 (sixfold higher in R than S, FDR <0.01, similar to AT1G27940 that encodes an auxin efflux transporter) met the criteria for significant differential expression but were excluded from the resistance hypothesis because both PRP39-2 and ABCB13 had at least one 2,4-D-resistant RIL replicate that deviated in expression pattern from the other replicates. Single-nucleotide polymorphism (SNP) calling was performed using SAMtools (version 1.3.1) with the default options and the "mpileup" command. The command "bcftools" was used to retain only SNPs that had a quality score higher than 10 and read depth higher than 10. An additional filtering step was performed for SNPs that were heterozygous or homozygous in at least three individuals of all R-RILs and all S-RILs. Contigs with annotations in the TIR1/AFB family and the Aux/IAA gene family were manually inspected for sequence variants between R-RILs and S-RILs using Integrative Genomics Viewer to view Binary Alignment Map file read alignments (42).

Sequence Verification of *IAA2* Deletion, Segregation, and Analysis of Field Populations. The *SoIAA2* deleted region was sequenced from samples of R-RILs and S-RILs used in RNA-seq. Complementary DNA (cDNA) was synthesized using iScript (Bio-Rad), and a PCR was performed with primers listed in *SI Appendix*, Table 6 spanning the predicted deletion in *IAA2*. Amplicons were Sanger sequenced. Transcript sequences of *SoIAA2* and $SoIAA2_{\Delta 27}$ were deposited in GenBank (accessions OK631624 and OK631625). To analyze the *IAA2* deletion in other resistant *S. orientale* populations collected in South Australia, plants were sprayed with 200 g/ai.ha^{-1} 2,4-D at the five true-leaf stage using an overhead track sprayer (DeVries Manufacturing) equipped with a flat-fan nozzle tip (Teejet 8002EVS, Spraying System) calibrated to deliver 187 L/ha^{-1} of spray solution at 172 kPa. Percent damage was evaluated at 28 DAT, and DNA was extracted by cetrimonium bromide (43) and analyzed using the primers listed in *SI Appendix*, Table 6 .

A progeny test segregation analysis was performed on 219 F3 plants derived from self-pollination of a heterozygous F2 individual from Cross B, identified via progeny test due to segregation of 2,4-D resistance in the F3. Plants were sprayed with 250 g/ai/ha^{-1} 2,4-D at the five true-leaf stage as described above, and visual injury was evaluated on a scale of 0% (no injury) to 100% (complete plant death). Kompetitive Allele Specific Polymerase Chain Reaction (KASP) genotyping markers were developed using a forward primer specific to the R (HEX) and S (FAM), together with a universal reverse primer (*SI Appendix*, Table 6).

Herbicide Absorption, Translocation, and Metabolism. *S. orientale* plants of both R and S genotypes were planted in soil under controlled conditions (60% relative humidity [RH], 21/18 °C, and 16/8 h light/dark photoperiod) and at the stage of two to three developed leaves, they were transferred to fine sand and irrigated with fertilizer. A total 1 wk later, the second true leaf was marked, covered with aluminum foil, and sprayed with a single nozzle overhead track sprayer (Generation III Research Sprayer; DeVries, Hollandale, MN) with 250 g/ha^{-1} 2,4-D (2,4-D amine; 455 g L-1; DuPont, Wilmington, DE) in a water volume of 224 L/ha^{-1} with 0.25% nonionic surfactant (NIS). The aluminum foil was removed, and a solution of [^{14}C] 2,4-D was applied in 10 droplets of 1 μL each, for total radioactivity applied per plant of 3.33 KBq (200,000 dpm). Three biological replicates were used for evaluation time points of 3, 6, 12, 24, 48, 96, and 192 h after herbicide treatment. At each time point, the treated leaf was cut and washed in 10% methanol and 1% NIS washing solution, and the rinse solution radioactivity was counted in 10 mL of scintillation mixture (Ecoscint XR, National Diagnostics, Atlanta, GA) using liquid scintillation spectrometry (Packard Tricarb 2300TR, Packard Instrument Co., Meriden, CT). Roots were removed from sand and washed with deionized water, and rinsate radioactivity was measured. Plants were then pressed on newspaper, dried in a 60 °C oven for 72 h, and exposed to Phosphor Screen film (GE Healthcare Life Sciences, Pittsburgh, PA), and images were taken 3 d later with a Typhoon Trio Imager (GE Healthcare). Subsequently, plants were separated into treated leaf, untreated leaves, stem, and roots and then oxidized in

a biological oxidizer (OX500; RJ Harvey Instrument Co., Tappan, NY) followed by radioactivity measurement.

For metabolism, the treated leaf and roots were washed, the entire plant was ground in liquid nitrogen and digested in 10 mL solution of acetic acid for 10 min, and this extraction was done three times. After filtering, the extract was concentrated using solid-phase extraction C18 cartridge, in 4 mL of acetonitrile, evaporated, and resuspended in 225 μL of HPLC. A solvent, filtered, and 200 μL of the solution was injected in the HPLC (Hitachi Instruments, Inc., San Jose, CA, and C18 Column, Zorbax Eclipse XDB-C18; Agilent Technologies, Santa Clara, CA; Mobile phase A: 89.9% water, 10% acetonitrile, and 0.1% formic acid; and phase B: 99.9% acetonitrile and 0.1% formic acid), attached to a radio detector (FlowStar LB 513; Berthold Technologies GmbH & Co., Bad Wildbad, Germany) with a flow-cell YG-150-U5D solid-cell YG-Scintillator (150 μl, Berthold Technologies). The proportion of absorbed, translocated, and metabolized herbicide was calculated using the equations from ref. 12, and the dataset was processed using the R package drc (44) to generate the corresponding mathematical models for each performed experiment (*SI Appendix*, Table 2).

Functional Validation of *IAA2* Deletion in *Arabidopsis*. *SoIAA2* alleles were amplified by PCR from cDNA (*SI Appendix*, Table 6), ligated into the binary vector *pFGC5941*, and transformed into *Agrobacterium tumefaciens* (strain GV3101). Each allele of *SoIAA2* was transformed into *Arabidopsis thaliana* (Col-0) by floral dip method (45). Seeds were plated on 1/2 MS, 1% phytoagar, and 7.5 $\mu g/mL^{-1}$ of ammonium glufosinate for selection of transformed seedlings. Homozygous plants of the subsequent generations containing one copy of the transgene were selected.

Root assays were performed in Plant Nutrient media (46) with 0.5% (wt/vol) sucrose and 0.6% agar, supplemented with synthetic and natural auxins (2,4-D, dicamba, and IAA, Caisson Labs). Seeds of *Arabidopsis* were gas sterilized, incubated at 4 °C in dark, plated directly in media with the respective treatment or ethanol as a control, and moved to a growth chamber with a yellow light filter after 3 d (60% RH, 21 °C, and continuous illumination). Roots were measured 7 d after the plates were moved to the growth conditions. Post-emergence dose responses with 2,4-D and dicamba were performed on preflowering 21-d-old homozygous transgenic plants for all constructs. Plants were harvested 21 d after treatment, dry mass was measured, and the dataset was processed using the R package drc (44) to generate dose–response models (*SI Appendix*, Table 3).

For gene-expression analysis under auxin treatments, soil-cultivated *S. orientale* (five to six leaves) and transgenic *Arabidopsis* lines (preflowering 16 leaves) were sprayed with 250 $g/ai/ha^{-1}$ 2,4-D, and at 6 h after treatment, a leaf disk was collected from the eighth leaf in *Arabidopsis* and fourth for *S. orientale*, cDNA was generated, and gene expression of known *Arabidopsis* auxin-responsive genes *GH3.3*, *AtIAA19*, and *AtIAA2* was analyzed by qPCR using primers listed in *SI Appendix*, Table 6.

In Silico Protein Structure Predictions. Susceptible (*So*IAA2) and resistant ($SoIAA2_{\Delta 9}$) protein sequences were used for IDR predictions using PrDos (47), IUPred (48), and Spot2 (49) algorithms. Kyte–Doolittle hydropathy maps were calculated by Expasy-linked ProtScale (50). The flexibility of the various portions of *So*IAA2 and $SoIAA2_{\Delta 9}$ was evaluated using Medusa (https://www.dsimb.inserm.fr/MEDUSA/) (51).

IAA2 Protein Purification. The cDNAs corresponding to the two alleles of *SoIAA2* were cloned into a pFN2A (GST) flexi vector (Promega; primers in *SI Appendix*, Table 6), expressed in *Escherichia coli* BL21, and purified using GST beads (Glutathione Sepharose 4B from GE) according to the manufacturer manual. The GST-IAA2 proteins were recovered, GST was cleaved using TEV protease (100 μL at 400 μM; New England Biolabs), and GST beads were added to eliminate GST and undigested proteins. The final purified *So*IAA2 and $SoIAA2_{\Delta 9}$ proteins were then quantified using spectrometry and separated on sodium dodecyl-sulfate polyacrylamide gel electrophoresis to verify the purity.

SEC Purification and Retention Volume Studies. The cleaved IAA2 proteins were loaded into a GE Superdex 200 10/300 increase column equilibrated in CD buffer (10 mM Tris H_2SO_4 pH 7.0 and 150 mM $NaClO_4$) and quantified using a Cary Bio-50 ultraviolet (UV)-Vis spectrophotometer. Proteins were quantified by a UV 280-nm detector. Protein oligomers were analyzed based on their retention volumes and compared to Bio-Rad gel filtration protein standards (15 to 600 kDa).

CD Analysis. CD was performed using a MOS-500 spectrometer (Bio-logic, France) scanning 185 to 265 nm with a 2-nm slit width at an acquisition rate of 2 s/nm^{-1}. Buffer and proteins were scanned in a polytetrafluoroethylene-stoppered 1-mm UV quartz cuvette (FireflySci). Protein concentration was between 1 and 7 μM, and the absorbance and photomultiplier tube voltage targeted were 1 AU and 500 V, respectively. CD measurements were taken three times, and the raw ellipticity values were averaged after buffer subtraction and converted to mean residue ellipticity or micromolar ellipticity values.

SPR Affinity Binding Analysis. SPR experiments were conducted according to the protocols described in Lee et al. (25) with modifications. TIR1/AFB5 was expressed in Sf9 insect cell culture using a recombinant baculovirus encoding 10xHis:GFP:FLAG:TEV:receptor and 10xHis:ASK1. Initial purification using the His-tag on nickel resin was followed by clean-up using FLAG chromatography. For SPR assays using a Biacore T200 (Cytiva), the purified protein was mixed with the appropriate concentration of each auxin before passing it over a streptavidin chip loaded with biotinylated *So*IAA2 and $SoIAA2_{\Delta 9}$ degron peptides (Thermo Fisher Scientific) (*SI Appendix*, Table 4).

The SPR buffer was Hepes-buffered saline (10 mM Hepes, 3 mM ethylenediaminetetraacetic acid, 150 mM NaCl, and 0.05% Tween 20). Binding experiments were run at a flow rate of 30 $\mu L/min^{-1}$ using a series of 100 s of injection and dissociation times, followed by a final dissociation of 600 s, according to the manufacturer's single-cycle kinetic routine. Data from a control channel (loaded with a mutated degron, mIAA7) (25) and from a buffer+DMSO-only run were subtracted from each sensogram following the standard double-reference subtraction protocol.

Homology-Based Modeling and Docking Analysis for TIR1 with *So*IAA2 and $SoIAA2_{\Delta 9}$. Homology models of portions of the sequences of *So*IAA2 corresponding to the PB1 domain and degron were aligned to chain C of PDB: 2P1Q (2) and PDB: 2M1M (4), respectively, using Praline (52). These crystal structures were used to generate homology models of the degron and PB1 portions of *So*IAA2 using Modeler (version 10.0) (53, 54). Homology models of portions of *So*IAA2 corresponding to the PB1 motif and degron motif portions were aligned on TIR1 from PDB:2P1Q using pymol, and the IDR segment connecting these two models was generated using ModLoop (55, 56). A similar process was followed to generate the $SoIAA2_{\Delta 9}$ version of this protein. Amino acids involved in the interaction between *So*IAA2 or $SoIAA2_{\Delta 9}$ and TIR1 were identified using the InterfaceResidues.py pymol script (https://pymolwiki.org/index.php/InterfaceResidues). These residues were used as docking parameters in high ambiguity driven protein-protein docking (HADDOCK) 2.4 (https://wenmr.science.uu.nl/haddock2.4/) (57–59). Docking calculations were performed under expert level, deactivating the DNA/RNA functions and activating the Surface Contact Restrains to enforce contact between the molecules. Degron residues KNNN of *So*IAA2 were assigned semiflexible properties during docking, whereas the shorter connection in $SoIAA2_{\Delta 9}$ was not allowed to be flexible to preserve the structural integrity of PB1. The binding affinities of the *So*IAA2/TIR1 and $SoIAA2_{\Delta 9}$/TIR1 biological complexes were calculated using protein binding energy prediction (PRODIGY) (https://bianca.science.uu.nl/prodigy/) (60, 61) for all top four poses from the best HADDOCK clusters.

Data Availability. RNA-sequencing data, transcript sequences, and protein docking calculations data have been deposited in NCBI GEO, NCBI GenBank, and Mountain Scholar [GEO Series accession no. GSE159202 (62); GenBank accessions OK631624 (63) and OK631625 (64); and Mountain Scholar DOI: https://dx.doi.org/10.25675/10217/234027 (65)].

ACKNOWLEDGMENTS. We thank Rachel Chayer for assistance with laboratory work. This work was supported in part by funding from Dow AgroSciences, by the Grains Research and Development Corporation—Australian Government, Grant UA00158, the Brazilian governmental scholarship from the National Council for Scientific and Technological Development (CNPq, 207387/2014-1) to M.R.A.d.F., and by the European Union Marie Skłodowska-Curie Actions Individual Fellowship project CrysPINs (792329) in support of M.F.K. R.N. and M.F.K. acknowledge equipment access at the Warwick Integrative Synthetic Biology Centre, which is funded by BB/M017982/1. The funders had no role in the conceptualization, design, data collection, analysis, decision to publish, or in preparation of the manuscript.

1. T. Ulmasov, Z. B. Liu, G. Hagen, T. J. Guilfoyle, Composite structure of auxin response elements. *Plant Cell* **7**, 1611–1623 (1995).
2. X. Tan *et al.*, Mechanism of auxin perception by the TIR1 ubiquitin ligase. *Nature* **446**, 640–645 (2007).
3. D. C. Dinesh, L. I. A. C. Villalobos, S. Abel, Structural biology of nuclear auxin action. *Trends Plant Sci.* **21**, 302–316 (2016).
4. D. C. Dinesh *et al.*, Solution structure of the *Ps*IAA4 oligomerization domain reveals interaction modes for transcription factors in early auxin response. *Proc. Natl. Acad. Sci. U.S.A.* **112**, 6230–6235 (2015).
5. M. Niemeyer *et al.*, Flexibility of intrinsically disordered degrons in AUX/IAA proteins reinforces auxin co-receptor assemblies. *Nat. Commun.* **11**, 2277 (2020).

6. M. A. Rinaldi, J. Liu, T. A. Enders, B. Bartel, L. C. Strader, A gain-of-function mutation in IAA16 confers reduced responses to auxin and abscisic acid and impedes plant growth and fertility. *Plant Mol. Biol.* **79**, 359–373 (2012).
7. K. Mockaitis, M. Estelle, Auxin receptors and plant development: A new signaling paradigm. *Annu. Rev. Cell Dev. Biol.* **24**, 55–80 (2008).
8. S. LeClere, C. Wu, P. Westra, R. D. Sammons, Cross-resistance to dicamba, 2,4-D, and fluroxypyr in *Kochia scoparia* is endowed by a mutation in an *AUX/IAA* gene. *Proc. Natl. Acad. Sci. U.S.A.* **115**, E2911–E2920 (2018).
9. C. Wu *et al.*, A dicamba resistance-endowing IAA16 mutation leads to significant vegetative growth defects and impaired competitiveness in kochia (Bassia scoparia)†. *Pest Manag. Sci.* **77**, 795–804 (2021).
10. I. Heap, The international survey of herbicide resistant weeds (2020). https://www.weedscience.com/. Accessed 22 April 2020.
11. T. A. Gaines *et al.*, Mechanisms of evolved herbicide resistance. *J. Biol. Chem.* **295**, 10307–10330 (2020).
12. M. R. Figueiredo *et al.*, Metabolism of 2,4-dichlorophenoxyacetic acid contributes to resistance in a common waterhemp (*Amaranthus tuberculatus*) population. *Pest Manag. Sci.* **74**, 2356–2362 (2018).
13. D. E. Goggin, G. R. Cawthray, S. B. Powles, 2,4-D resistance in wild radish: Reduced herbicide translocation via inhibition of cellular transport. *J. Exp. Bot.* **67**, 3223–3235 (2016).
14. D. J. Pettinga *et al.*, Increased chalcone synthase (CHS) expression is associated with dicamba resistance in *Kochia scoparia*. *Pest Manag. Sci.* **74**, 2306–2315 (2018).
15. D. E. Goggin, S. Bringans, J. Ito, S. B. Powles, Plasma membrane receptor-like kinases and transporters are associated with 2,4-D resistance in wild radish. *Ann. Bot.* **125**, 821–832 (2020).
16. O. E. Todd *et al.*, Synthetic auxin herbicides: Finding the lock and key to weed resistance. *Plant Sci.* **300**, 110631 (2020).
17. C. Preston, F. C. Dolman, P. Boutsalis, Multiple resistance to acetohydroxyacid synthase–inhibiting and auxinic herbicides in a population of oriental mustard (*Sisymbrium orientale*). *Weed Sci.* **61**, 185–192 (2013).
18. H. T. Dang *et al.*, Reduced translocation in 2,4-D-resistant oriental mustard populations (*Sisymbrium orientale* L.) from Australia. *Pest Manag. Sci.* **74**, 1524–1532 (2018).
19. C. Preston, J. M. Malone, Inheritance of resistance to 2,4-D and chlorsulfuron in a multiple-resistant population of *Sisymbrium orientale*. *Pest Manag. Sci.* **71**, 1523–1528 (2015).
20. T. R. Wright *et al.*, Robust crop resistance to broadleaf and grass herbicides provided by aryloxyalkanoate dioxygenase transgenes. *Proc. Natl. Acad. Sci. U.S.A.* **107**, 20240–20245 (2010).
21. M. R. Behrens *et al.*, Dicamba resistance: Enlarging and preserving biotechnology-based weed management strategies. *Science* **316**, 1185–1188 (2007).
22. M. H. Nanao *et al.*, Structural basis for oligomerization of auxin transcriptional regulators. *Nat. Commun.* **5**, 3617 (2014).
23. J. Kim, K. Harter, A. Theologis, Protein–protein interactions among the Aux/IAA proteins. *Proc. Natl. Acad. Sci. U.S.A.* **94**, 11786–11791 (1997).
24. A. Micsonai *et al.*, BeStSel: A web server for accurate protein secondary structure prediction and fold recognition from the circular dichroism spectra. *Nucleic Acids Res.* **46** (W1), W315–W322 (2018).
25. S. Lee *et al.*, Defining binding efficiency and specificity of auxins for SCF($^{TIR1/AFB}$)-Aux/IAA co-receptor complex formation. *ACS Chem. Biol.* **9**, 673–682 (2014).
26. L. I. A. Calderón Villalobos *et al.*, A combinatorial TIR1/AFB-Aux/IAA co-receptor system for differential sensing of auxin. *Nat. Chem. Biol.* **8**, 477–485 (2012).
27. A. Waterhouse *et al.*, SWISS-MODEL: Homology modelling of protein structures and complexes. *Nucleic Acids Res.* **46** (W1), W296–W303 (2018).
28. D. A. Korasick *et al.*, Molecular basis for AUXIN RESPONSE FACTOR protein interaction and the control of auxin response repression. *Proc. Natl. Acad. Sci. U.S.A.* **111**, 5427–5432 (2014).
29. X. Yang *et al.*, The IAA1 protein is encoded by AXR5 and is a substrate of SCF(TIR1). *Plant J.* **40**, 772–782 (2004).
30. Y. Yang, X. Zhang, B. Yu, O-Glycosylation methods in the total synthesis of complex natural glycosides. *Nat. Prod. Rep.* **32**, 1331–1355 (2015).
31. P. Nagpal *et al.*, *AXR2* encodes a member of the Aux/IAA protein family. *Plant Physiol.* **123**, 563–574 (2000).
32. Q. Tian, J. W. Reed, Control of auxin-regulated root development by the *Arabidopsis thaliana SHY2/IAA3* gene. *Development* **126**, 711–721 (1999).
33. L. E. Rogg, J. Lasswell, B. Bartel, A gain-of-function mutation in *IAA28* suppresses lateral root development. *Plant Cell* **13**, 465–480 (2001).
34. R. Edgar, M. Domrachev, A. E. Lash, Gene Expression Omnibus: NCBI gene expression and hybridization array data repository. *Nucleic Acids Res.* **30**, 207–210 (2002).
35. W. Li, A. Godzik, Cd-hit: A fast program for clustering and comparing large sets of protein or nucleotide sequences. *Bioinformatics* **22**, 1658–1659 (2006).
36. B. J. Haas *et al.*, De novo transcript sequence reconstruction from RNA-seq using the Trinity platform for reference generation and analysis. *Nat. Protoc.* **8**, 1494–1512 (2013).
37. T. Z. Berardini *et al.*, The Arabidopsis information resource: Making and mining the "gold standard" annotated reference plant genome. *Genesis* **53**, 474–485 (2015).
38. B. Langmead, S. L. Salzberg, Fast gapped-read alignment with Bowtie 2. *Nat. Methods* **9**, 357–359 (2012).
39. H. Li *et al.*; 1000 Genome Project Data Processing Subgroup, The sequence alignment/map format and SAMtools. *Bioinformatics* **25**, 2078–2079 (2009).
40. M. D. Robinson, D. J. McCarthy, G. K. Smyth, edgeR: A bioconductor package for differential expression analysis of digital gene expression data. *Bioinformatics* **26**, 139–140 (2010).
41. R Core Team, R: A language and environment for statistical computing. R Foundation for Statistical Computing, Vienna, Austria (2021). https://www.R-project.org/. Accessed 18 February 2022.
42. H. Thorvaldsdóttir, J. T. Robinson, J. P. Mesirov, Integrative Genomics Viewer (IGV): High-performance genomics data visualization and exploration. *Brief. Bioinform.* **14**, 178–192 (2013).
43. J. J. Doyle, J. L. Doyle, A rapid DNA isolation procedure for small quantities of fresh leaf tissue. *Phytochem. Bull.* **19**, 11–15 (1987).
44. S. Z. Knezevic, J. C. Streibig, C. Ritz, Utilizing R software package for dose-response studies: The concept and data analysis. *Weed Technol.* **21**, 840–848 (2007).
45. S. J. Clough, A. F. Bent, Floral dip: A simplified method for *Agrobacterium*-mediated transformation of *Arabidopsis thaliana*. *Plant J.* **16**, 735–743 (1998).
46. G. W. Haughn, C. Somerville, Sulfonylurea-resistant mutants of *Arabidopsis thaliana*. *Mol. Gen. Genet.* **204**, 430–434 (1986).
47. T. Ishida, K. Kinoshita, PrDOS: Prediction of disordered protein regions from amino acid sequence. *Nucleic Acids Res.* **35**, W460–W464 (2007).
48. B. Mészáros, G. Erdős, Z. Dosztányi, IUPred2A: Context-dependent prediction of protein disorder as a function of redox state and protein binding. *Nucleic Acids Res.* **46** (W1), W329–W337 (2018).
49. J. Hanson, Y. Yang, K. Paliwal, Y. Zhou, Improving protein disorder prediction by deep bidirectional long short-term memory recurrent neural networks. *Bioinformatics* **33**, 685–692 (2017).
50. E. Gasteiger *et al.*, "Protein identification and analysis tools on the ExPASy server" in *The Proteomics Protocols Handbook*, J. M. Walker, Ed. (Humana Press, Totowa, NJ, 2005), pp. 571–607.
51. Y. Vander Meersche, G. Cretin, A. G. de Brevern, J.-C. Gelly, T. Galochkina, MEDUSA: Prediction of protein flexibility from sequence. *J. Mol. Biol.* **433**, 166882 (2021).
52. V. A. Simossis, J. Heringa, PRALINE: A multiple sequence alignment toolbox that integrates homology-extended and secondary structure information. *Nucleic Acids Res.* **33**, W289–W294 (2005).
53. B. Webb, A. Sali, Comparative protein structure modeling using MODELLER. *Curr. Protoc. Bioinformatics* **47**, 5.6.1–5.6.32 (2014).
54. B. Webb, A. Sali, "Protein structure modeling with MODELLER" in *Functional Genomics: Methods in Molecular Biology*, M. Kaufmann, C. Klinger, A. Savelsbergh, Eds. (Humana Press, New York, NY, 2017), **vol. 1654**, pp. 39–54.
55. A. Fiser, R. K. Do, A. Sali, Modeling of loops in protein structures. *Protein Sci.* **9**, 1753–1773 (2000).
56. A. Fiser, A. Sali, ModLoop: Automated modeling of loops in protein structures. *Bioinformatics* **19**, 2500–2501 (2003).
57. S. J. de Vries, M. van Dijk, A. M. J. J. Bonvin, The HADDOCK web server for data-driven biomolecular docking. *Nat. Protoc.* **5**, 883–897 (2010).
58. J. Roel-Touris, C. G. Don, R. V Honorato, J. P. G. L. M. Rodrigues, A. M. J. J. Bonvin, Less is more: Coarse-grained integrative modeling of large biomolecular assemblies with HADDOCK. *J. Chem. Theory Comput.* **15**, 6358–6367 (2019).
59. G. C. P. van Zundert *et al.*, The HADDOCK2.2 web server: User-friendly integrative modeling of biomolecular complexes. *J. Mol. Biol.* **428**, 720–725 (2016).
60. L. C. Xue, J. P. Rodrigues, P. L. Kastritis, A. M. Bonvin, A. Vangone, PRODIGY: A web server for predicting the binding affinity of protein-protein complexes. *Bioinformatics* **32**, 3676–3678 (2016).
61. A. Vangone, A. M. J. J. Bonvin, Contacts-based prediction of binding affinity in protein-protein complexes. *eLife* **4**, e07454 (2015).
62. M. R. A. Figueiredo *et al.*, Resistance to the herbicide 2,4-D in *Sisymbrium orientale* conferred by a deletion mutation in the degron tail of IAA2. Gene Expression Omnibus. https://www.ncbi.nlm.nih.gov/geo/query/acc.cgi?acc=GSE159202. Deposited 7 October 2020.
63. M. R. A. Figueiredo *et al.*, An in-frame deletion mutation in the degron tail of auxin co-receptor IAA2 confers resistance to the herbicide 2,4-D in *Sisymbrium orientale*. NCBI GenBank. https://www.ncbi.nlm.nih.gov/nuccore?term=OK631624. Deposited 21 October 2021.
64. M. R. A. Figueiredo *et al.*, An in-frame deletion mutation in the degron tail of auxin co-receptor IAA2 confers resistance to the herbicide 2,4-D in *Sisymbrium orientale*. NCBI GenBank. https://www.ncbi.nlm.nih.gov/nuccore?term=OK631625. Deposited 21 October 2021.
65. M. R. A. Figueiredo *et al.*, An in-frame deletion mutation in the degron tail of auxin co-receptor IAA2 confers resistance to the herbicide 2,4-D in *Sisymbrium orientale*. Mountain Scholar Digital Repository. 10.25675/10217/234027. Deposited 26 October 2021.